PERGAMON

International Journal of Heat and Mass Transfer 42 (1999) 3047–3056

International Journal of HEAT and MASS TRANSFER

Local heat transfer measurements of an orthogonally rotating square duct with angled rib turbulators

Akira Murata[a,*], Sadanari Mochizuki[b], Tatsuji Takahashi[b]

[a]*Graduate School of Bio-Applications and Systems Engineering, Tokyo University of Agriculture and Technology, 2-24-16 Nakacho, Koganei, Tokyo 184-8588, Japan*

[b]*Department of Mechnical Systems Engineering, College of Engineering, Tokyo University of Agriculture and Technology, 2-24-16 Nakacho, Koganei, Tokyo 184-8588, Japan*

Received 29 June 1998; received in revised form 10 December 1998

Abstract

The effect of angled rib turbulators on the heat transfer of an orthogonally rotating square duct were experimentally investigated. The Reynolds and rotation numbers were varied in 10,000–20,000 and 0–0.08, respectively. The leading and trailing walls were rib-roughened with angles of 90° and 60°. The results showed that the rotation induced a peripheral variation of the heat transfer and the higher heat transfer was seen using the 60° angled rib; judging from the local heat transfer variation, the skewed secondary flow induced by the angled rib seemed to result in additional heat transfer enhancement. © 1999 Elsevier Science Ltd. All rights reserved.

1. Introduction

In the development of high performance gas turbines, effective blade cooling is essential because the higher efficiency of the turbine requires a higher inlet gas temperature. Generally, this blade cooling is performed by film cooling at the external surface of the turbine blade and also by internal forced-convection cooling which uses winding flow passages inside the turbine blade. In the internal forced-convection cooling, the real phenomena are made very complicated by external forces: the Coriolis force and the buoyancy force in the centrifugal acceleration field. In addition to these external forces, the effects induced by a 180° sharp turn and turbulence promoters (ribs) installed on the internal surface result in phenomena that are far from understood [1].

When the previous studies which conducted spatial variation measurement of local heat transfer coefficients in a rib-roughened duct are reviewed, it can be seen that various techniques have been applied to the measurement of local heat transfer: wall temperature measurement using hundreds of thermocouples [2], local mass transfer measurement using a naphthalene sublimation technique [3], and wall temperature measurement using temperature-sensitive liquid crystal [4–6], although every study was for a stationary condition. The number of previous experimental studies which measured spatial variation of local heat transfer coefficients of a rotating rib-roughened duct is limited. Moreover, as shown in Fig. 1, the relative direction between the main flow and the buoyancy force changes depending on the radial flow direction, and, therefore, the heat transfer characteristics must also be affected

* Corresponding author.

0017-9310/99/$ - see front matter © 1999 Elsevier Science Ltd. All rights reserved.
PII: S0017-9310(99)00004-6

Nomenclature

d_e	hydraulic diameter (= 14 mm)
d^+	dimensionless diameter of the tripping wire ($= du_*/\nu$)
Gr	Grashof number ($= r\omega^2\beta d_e^4\dot{q}/(\lambda\nu^2)$)
h	heat transfer coefficient
Nu	Nusselt number ($= hd_e/\lambda$)
Pr	Prandtl number
$\dot{q}$	wall heat flux
r	mean rotation radius (= 330 mm)
Ra	Rayleigh number ($= GrPr$)
Re	Reynolds number ($= U_m d_e/\nu$)
Ro	rotation number ($= \omega d_e/U_m$)
T_w	wall temperature
T_b	bulk temperature
u_*	friction velocity
U_m	mean velocity
z	streamwise coordinate

Greek symbols

β	coefficient of thermal expansion
ϕ	rib angle
λ	thermal conductivity
ν	kinematic viscosity
ω	angular velocity

Subscripts

L	local value
m	duct average
w	wall
0–z	averaged in region of $z = 0$–z
7–8	averaged in region of $z/d_e = 7$–8
∞	fully developed

by this radial flow direction; however, there has been no previous study which examined the effect of the radial flow direction with the same inlet condition for both radially inward and outward flows.

In previous numerical studies, several researchers treated turbulent flow in a rotating condition: a rotating smooth duct using the k–ϵ two equation model or the algebraic equation model [7] and a rotating rib-roughened duct using the k–ϵ two equation model [8]. Although the approach using the Reynolds average turbulence models could reproduce the heat transfer of the blade cooling to a certain extent, the turbulence model itself includes empirical constants and functions which have to be optimized depending on the flow field. As Launder et al. [9] pointed out, it should be noted that in order to quantitatively simulate the flow in a rotating system, the second moment closure, that is, the Reynolds stress equation model, is a minimum requirement.

This research is a continuation of research on heat transfer measurement by using thermocouples in various configurations: stationary smooth [10] and rib-roughened [2] ducts with a 180° sharp turn, rotating smooth [11] and rib-roughened [12] ducts with a 180° sharp turn, and a rotating smooth straight duct [13]. This study deals with the heat transfer of a rotating rib-roughened square straight duct with rib angles of 90° and 60°. The rib angle of 90° is chosen as a basic configuration, and that of 60° is chosen because it gave the best heat transfer performance in the previous experiments [2]. Comparing the results between smooth and rib-roughened ducts, the effects of the rib installation and then the rib angle on the heat transfer are examined. In addition, experiments are performed changing the radial flow direction in inward and outward flows in order to investigate the effect of the relative direction between the buoyancy force and the main stream.

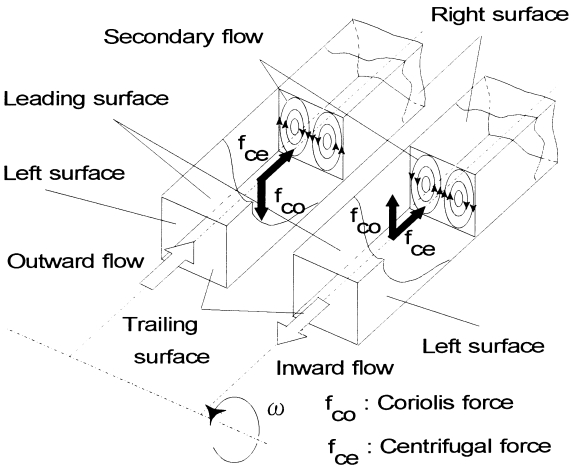

Fig. 1. Effects of Coriolis and centrifugal forces on the flow in an orthogonally rotating duct.

2. Experiments

Fig. 2 shows a schematic of the experimental apparatus. First, the radially inward flow configuration will be explained. Air sucked by using a turbo blower (1) was conditioned by passing through an entrance section consisting of a honeycomb, meshes, and a contraction in which the cross section changed from 44×44 mm^2 to 14×14 mm^2 in a length of 35 mm. The air from the entrance section flowed into a test section (3) with a uniform velocity profile. The uniform velocity profile was chosen as an inlet condition in order to maintain the same inlet condition for both radially inward and outward flows in a relatively short length at the entrance section because the total length of the flow passage was limited by a short mean rotating radius, $r = 330$ mm. At the end of the entrance section (15 mm upstream from the location where heating was started), tripping wires, of which diameter was 0.8 mm or $d^+ = 66$ for a Reynolds number of 20,000, were installed normal to the duct axis on every four walls in order to turbulate the relaminarized flow because of the accelerating flow condition at the entrance contraction. The air exiting the test section turned its flow direction by 90° and was exhausted to a stationary piping system through a hollow rotating shaft and a rotary seal. The flow rate of air was measured by using a laminar flowmeter (2) and a manometer (4). The test section made of 5 mm thick Bakelite plates was a straight duct with a square cross section. The heat transfer surfaces consisted of a 200 μm thick plastic sheet (an electrically conductive surface layer of 20 μm in thickness) pasted on four inner surfaces. In order to thermally insulate the test section, the outer surface of the test section was covered by insulation materials. By passing an electric current through the conductive layer of the plastic sheet, a uniform heat flux condition was obtained. The wall temperatures were measured by using K-type thermocouples with a diameter of 50 μm. After a steady condition was attained in both the flow and temperature fields, an electronic circuit on the rotating system connected a selected thermocouple line to a microcomputer (6) via a mercury slip ring (5). The connected thermocouple line was switched as the system rotated. At one measurement location, 50 data points were measured and used to give an average value. When the radially outward flow was examined,

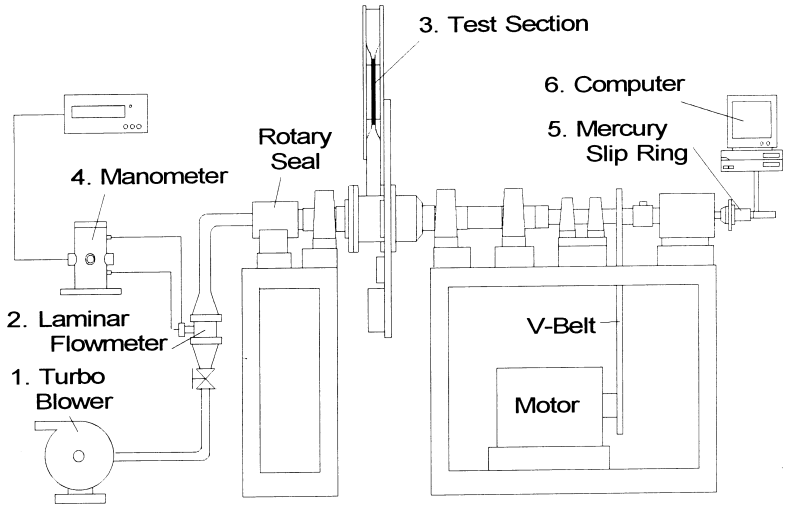

Fig. 2. Experimental apparatus schematic.

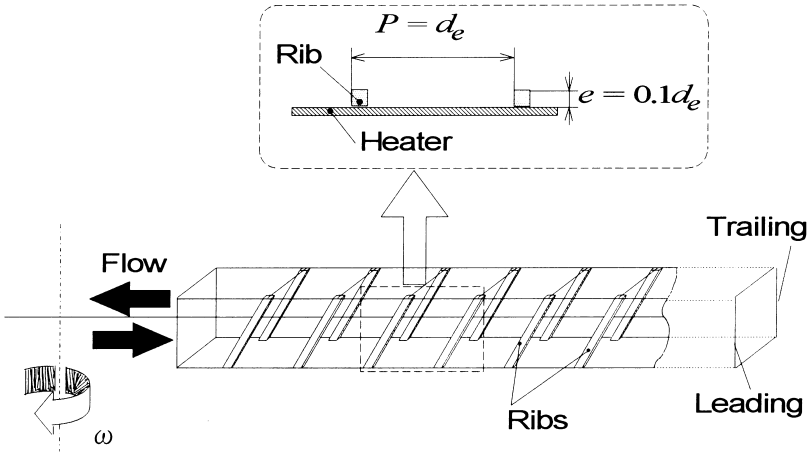

Fig. 3. Test section schematic.

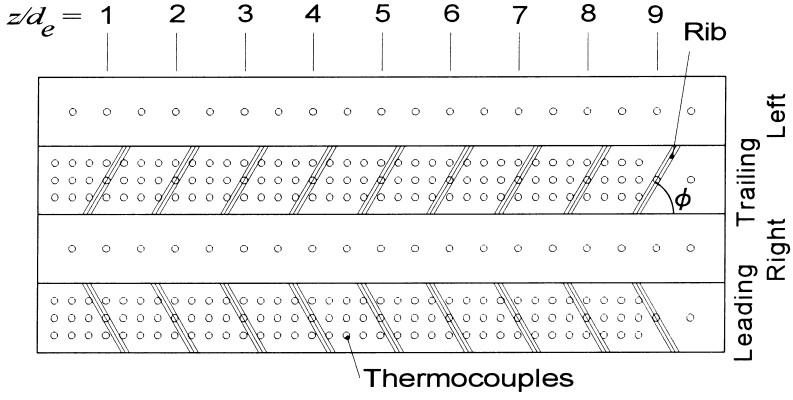

(a) Overall view of thermocouple locations on four walls

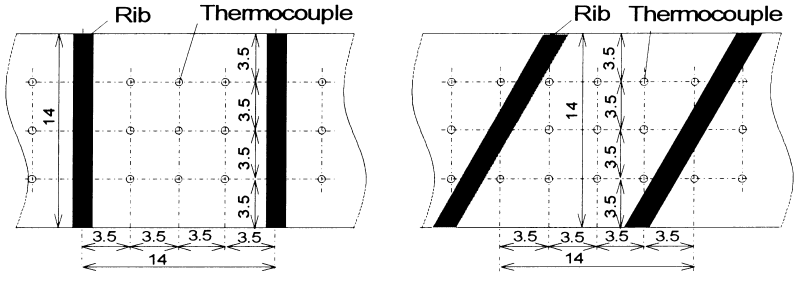

(b) 90° rib-roughened wall (c) 60° rib-roughened wall

Fig. 4. Location of thermocouples on the heating walls.

the test section was installed reversely on the rotating stage, and the turbo blower was used to blow in the air.

Fig. 3 shows a schematic of the test section. The test section with a square cross section is a five times scale-up model of a straight section of a cooling flow passage in a real gas turbine blade: the side length was 14 mm which was equal to a hydraulic diameter, d_e, and the streamwise length was 140 mm. Turbulence promoters (ribs) were installed symmetrically with a streamwise pitch of d_e on the two opposite heating surfaces, that is, the leading and trailing surfaces. There remained a small gap of 0.5 mm between the smooth side wall and the rib edge in the rib installation. The rib which was made of Bakelite had a square cross section with side length of 1.4 mm which is equivalent to 116 when normalized by using an inner scale, ν/u_*, for a Reynolds number of 20,000. This rib configuration of the rib height-to-hydraulic diameter ratio, 0.1, and the rib pitch-to-hydraulic diameter ratio, 1.0, was chosen to be within the previously observed optimal values of the rib arrangement [14,15]. As shown in Fig. 4, the thermocouples were installed with a transverse pitch of 3.5 mm (3) points) and a streamwise pitch of 3.5 mm on the leading and trailing walls; on the side (right and left) walls, the thermocouples were installed only at the transverse center with a streamwise pitch of 7.0 mm. The total number of the thermocouples used for the wall temperature measurement was 252, although the thermocouples located beneath the ribs were excluded in the data analysis.

The experiments were performed with and without rib installation and for radially inward and outward flow configurations. The Reynolds number, Re, the rotation number, Ro, and the Rayleigh number, Ra, are defined as follows:

$$Re = \frac{U_m d_e}{\nu}, \tag{1}$$

$$Ro = \frac{\omega d_e}{U_m}, \tag{2}$$

$$Ra = \frac{r\omega^2 \beta d_e^4 \dot{q} Pr}{\lambda \nu^2} (= GrPr). \tag{3}$$

In this study, the Reynolds number defined by using the mean velocity, U_m, and the hydraulic diameter, d_e, was varied in $Re = 10{,}000$, 15,000, and 20,000, the rotation number $Ro = 0$–0.08, and the Rayleigh number $Ra = 1.8 \times 10^7$–8.8×10^7; maximum values were expressed with dimension as $U_m = 22$ m/s and a rotation speed of 600 rpm.

The Nusselt number was calculated as follows:

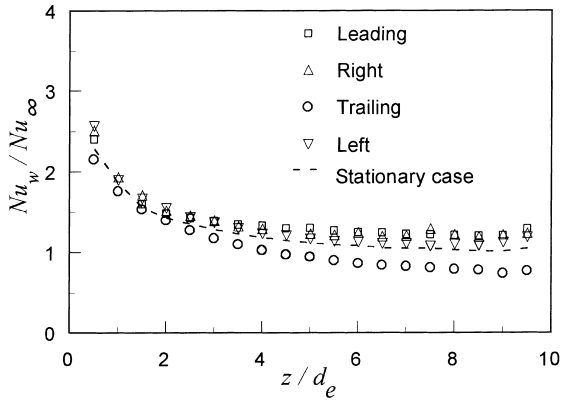

Fig. 5. Streamwise variation of transversely averaged Nusselt number (inward flow, $Re = 15{,}000$, $Ro = 0.052$ (600 rpm), $Ra = 8.8 \times 10^7$).

$$Nu = \frac{h d_e}{\lambda} = \frac{\dot{q} d_e}{\lambda (T_w - T_b)}. \tag{4}$$

The properties were calculated by using the film temperatures.

In order to estimate the heat loss from the outer surface of the test section, the outer surface temperatures were measured at the transverse center by using thermocouples installed with a streamwise pitch of 21 mm (7 points) on the outer surface of each wall. Using the outer surface temperatures and the interpolated heat-transfer-surface temperature corresponding to the outer surface measurement location, the estimated heat loss was calculated with the assumption of one-dimensional heat conduction in the test section wall. This heat loss was less than 5% of the heat input for the case of $Re = 20{,}000$. The averaged Nusselt number was calculated by using the integral average temperature difference on the surface area in question. The Nusselt number in the figure of this study was normalized by using the following values for the fully developed turbulent pipe flow [16]:

$$Nu_\infty = 0.022 Re^{0.8} Pr^{0.5}. \tag{5}$$

The measurement uncertainty [17] was estimated for the representative value of $Nu/Nu_\infty = 2$ to have about $\pm 5\%$ with a confidence level of 95%.

3. Results and discussion

3.1. Case of a smooth duct (without ribs)

Fig. 5 shows the streamwise variation of the transversely averaged Nusselt number, Nu_w, of the inward flow case. The horizontal axis is a dimensionless

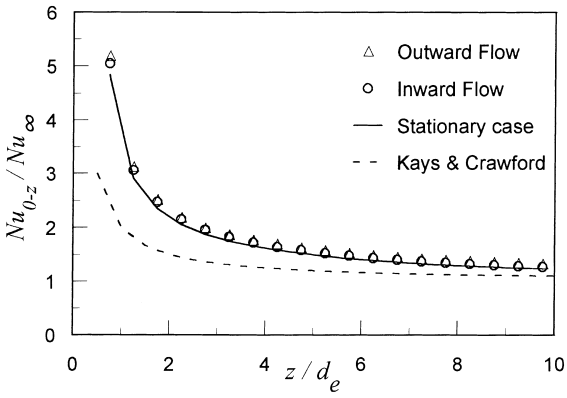

Fig. 6. Comparison of flow direction in streamwise variation of Nusselt number averaged in both peripheral and streamwise directions from the entrance to z ($Re = 15{,}000$, $Ro = 0.052$ (600 rpm), $Ra = 8.8 \times 10^7$).

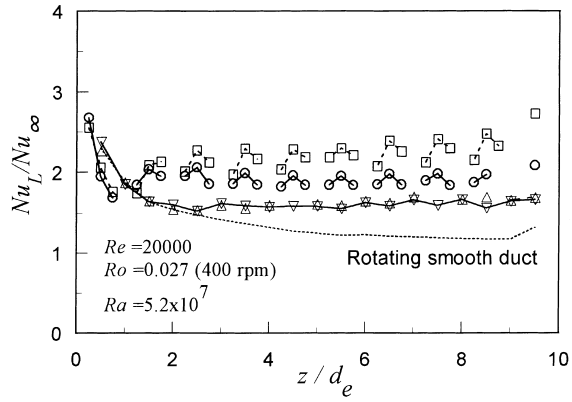

Fig. 7. Streamwise variation of local Nusselt number for 90° rib duct (□: leading, ○: trailing, △: right, ▽: left).

streamwise location, z/d_e, and the broken line in the figure shows the peripherally averaged Nusselt number of the stationary case. When the plotted data are compared with the stationary result of the broken line in the downstream region, the Nusselt numbers on the leading and trailing walls show higher and lower values, respectively. This heat transfer variation is considered to be caused by the Coriolis induced secondary flow which makes the boundary layer on the pressure (leading) side thinner and therefore the Nusselt number higher [13]. On the other hand, the boundary layer on the suction (trailing) side becomes thicker and therefore the Nusselt number lower. In the case of the radially outward flow, the direction of the Coriolis force is reversed; therefore, the behavior of the Nusselt numbers on the leading and trailing walls was reversed (not shown here).

Fig. 6 shows the streamwise variation of the Nusselt number averaged in both peripheral and streamwise directions from the entrance to the streamwise location, z. In the figure, the solid and broken lines are for Nu_{0-z} of the stationary case and the empirical value of the fluid-dynamically and thermally developing turbulent pipe flow [18], respectively. For both stationary and rotating cases, Nu_{0-z} of this study is higher than the empirical value shown as 'Kays & Crawford' in the figure because the tripping wires introduce turbulence into the flow at the entrance. However, in the downstream region, the tendency to approach the empirical value is seen. In the rotating case, Nu_{0-z} shows almost the same value as that of the stationary case, and the difference in Nu_{0-z} between the radially inward and outward flow cases is only 3%. When the Nusselt number results are examined in the local value, the Nusselt number gives higher and lower values on the pressure and suction surfaces, respectively. However, the peripherally averaged value does not show a discernible difference from the stationary case, because the peripheral variation in the local value compensates for each other. In the present experiments, the radial flow direction did not give a discernible difference in Nu_{0-z} (see also Fig. 13 in section 3.4.) possibly because of the following two reasons: the developing flow condition and the relatively small value of the Rayleigh number ($Gr/Re^2 < 0.55$), which was limited by the highest attainable temperature of the conductive plastic sheet (about 120°). Therefore, in the following sections, the results of the radially inward flow case will mainly be discussed unless otherwise noted.

3.2. Case of a 90° rib-roughened duct

Fig. 7 shows the streamwise variation of the local

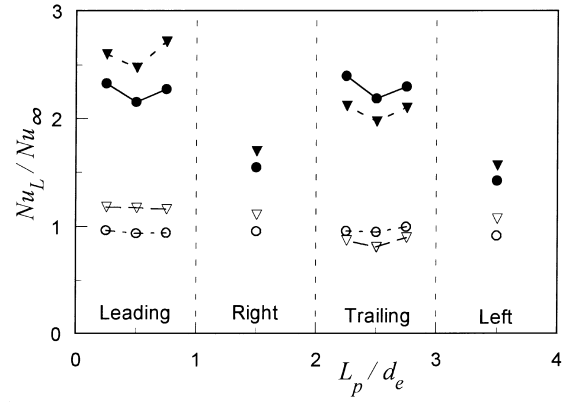

Fig. 8. Peripheral variation of local Nusselt number ($Re = 20{,}000$, black and white symbols are for 90° rib and smooth ducts, respectively; ●○: stationary, ▼▽: $Ro = 0.026$ (400 rpm), $Ra = 5.1 \times 10^7$, $z/d_e = 8.5$).

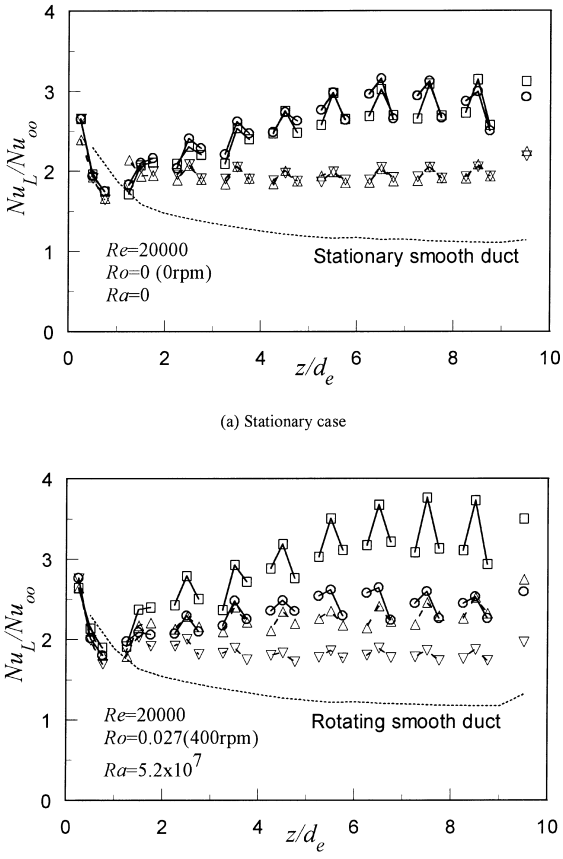

(a) Stationary case

(b) Rotating case

Fig. 9. Streamwise variation of local Nusselt number at transverse center (□: 60° leading, ○: 60° trailing, △: 90° leading, ▽: 90° trailing).

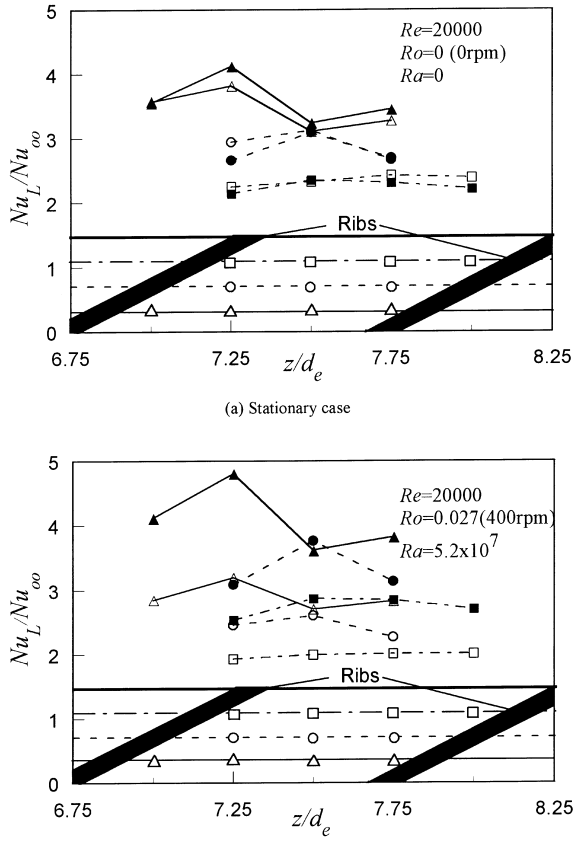

(a) Stationary case

(b) Rotating case

Fig. 10. Variation of local Nusselt number between two consecutive ribs at $z/d_e = 7$–8 (black and white symbols are for leading and trailing walls, respectively; ■□: left side, ●○: center, ▲△: right side).

Nusselt number, Nu_L, for the 90° rib configuration. The dotted line in the figure shows the peripherally averaged value of a rotating smooth duct. For the leading and trailing walls, only the value at the transverse center is shown. When the ribs are installed, the heat transfer on all four walls is enhanced as compared to the smooth duct case. On the rib-roughened leading and trailing walls, Nu_L gives locally maximum values between the consecutive ribs and shows streamwise periodicity. Between the consecutive ribs, the flow separation and its reattachment induced by the upstream rib result in a locally maximum Nusselt number and also affect the heat transfer on the side (right and left) walls [5]. When the Nusselt number on the leading and trailing walls are compared, the pressure (leading) surface gives the higher Nu_L; this is similar to the smooth duct case.

Fig. 8 shows the peripheral variation of the local Nusselt number, Nu_L, at the downstream location of $z/d_e = 8.5$. The result of the rib-roughened case gives a higher value than that of the smooth duct. For the rib-roughened case, Nu_L at the transverse center is lower than at the other two locations on the leading and trailing walls; for the smooth duct case, however, this tendency is only slightly observed on the trailing surface. As seen in the smooth duct case, due to the effect of the Coriolis force for the rotating case, Nu_L on the pressure and suction surfaces increases and decreases, respectively. On the right and left walls, the Nu_L also increases because of the rotation.

3.3. Case of a 60° angled rib-roughened duct

Fig. 9 shows the streamwise variation of the local Nusselt number at the transverse center of leading and trailing walls. In the stationary case of Fig. 9(a), the 60° rib-roughened duct gives a local maximum value at the mid-point between the consecutive ribs and this situation repeats in the streamwise direction. Nu_L of

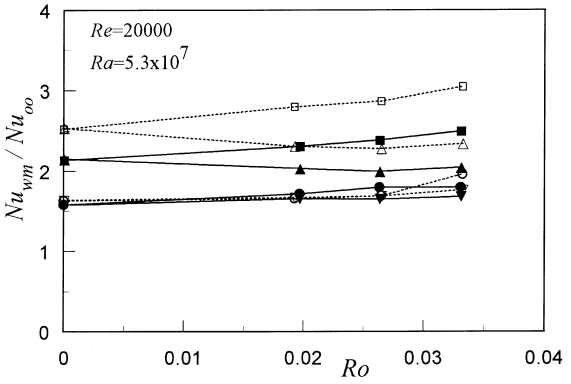

Fig. 11. Effects of rib angle and Coriolis force on wall-averaged Nusselt numbers (black and white symbols are for 90° and 60° cases, respectively; ■□: leading, ●○: right, ▲△: trailing, ▼▽: left).

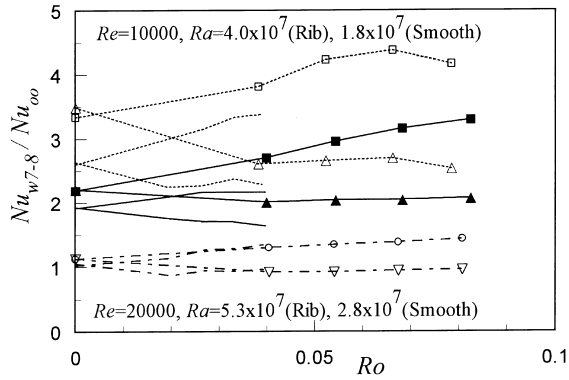

Fig. 12. Effects of rib angle and Coriolis force on wall-averaged Nusselt numbers at downstream region, $z/d_e = 7$–8 (symbols, ○■□: leading and ▽▲△: trailing, are for smooth, 90° rib, and 60° rib cases of $Re = 10{,}000$, respectively; for $Re = 20{,}000$, only lines are drawn with the same line type as that of $Re = 10{,}000$).

the 60° rib-roughened duct is larger than that of the 90° rib-roughened duct. In the stationary 90° rib case, the periodicity becomes steady at around $z/d_e = 2$–3; on the other hand, in the stationary 60° rib case, Nu_L gradually increases in the streamwise direction. This gradual change can be due to an additional secondary flow induced by the angled rib along which the velocity component is induced [4]. As shown in Fig. 9(b), the higher value on the pressure (leading) surface than the suction (trailing) surface is the same as the situation of the smooth duct and the 90° rib-roughened duct. When the duct rotates, the flow development behavior becomes more complicated because of two factors which induce the secondary flow: the angled rib and the Coriolis force.

Fig. 10 shows the variation of the local Nusselt number on the leading and trailing walls between two consecutive ribs at $z/d_e = 7$–8. It should be noted that in the schematic drawing of the figure the rib angle seems larger because the horizontal and vertical scales are not matched in the drawing. In the stationary case of Fig. 10(a), Nu_L of the right side is the largest and followed by that of the center and then the left side. When compared between these data at three different transverse locations, the location of the local maximum moves to a downstream location and can be listed starting from the upstream location in the same order as the above-mentioned level of Nu_L: the right side, the center, and the left side. The fluid near the rib-roughened wall tends to flow along the angled rib direction, and, therefore, the rib-angle induced flow component must appear. The left side corresponds to the downstream location from the viewpoint of this rib-angle induced secondary flow; thus, Nu_L of the left side becomes the smallest in Fig. 10(a) [4]. In the rotating case of Fig. 10(b), due to the Coriolis induced secondary flow, Nu_L on the leading and trailing walls increases and decreases, respectively; however, the qualitative tendency is similar to that of the stationary case.

3.4. Comparison in wall-averaged and duct-averaged values

Fig. 11 shows the relation between the wall-averaged Nusselt number, Nu_{wm}, and the rotation number, Ro. Here, Nu_{wm} is averaged on each wall in both transverse and streamwise directions from the entrance to the exit of the test section. According to the increase in Ro, Nu_{wm} on the leading and trailing walls increases and decreases, respectively, as a consequence of the similar tendency seen in the local Nusselt numbers.

Fig. 12 shows the result of the wall-averaged Nusselt number, Nu_{w7-8}, at the downstream region of $z/d_e = 7$–

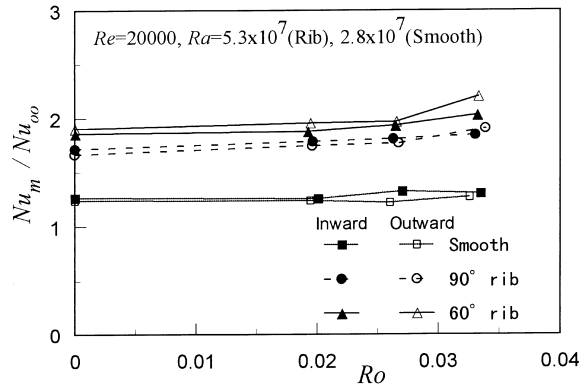

Fig. 13. Effect of rotation, rib angle, and radial flow direction on overall Nusselt number.

8. In the figure, the plotted symbols with lines are for $Re = 10{,}000$, and the lines alone are drawn in the region of $Ro \leqslant 0.04$ for $Re = 20{,}000$. This average in the region of $z/d_e = 7$–8 aims at the approximately developed value, and the results are almost similar to that of Fig. 11. The heat transfer enhancement is larger for the lower Reynolds number case ($Re = 10{,}000$).

Fig. 13 shows the relation between the duct-averaged Nusselt number, Nu_m, and the rotation number, Ro, for $Re = 20{,}000$. When the duct-averaged Nusselt numbers are compared among the rib configurations examined, Nu_m becomes larger in the following descending order: the 60° angled rib-roughened duct, the 90° rib-roughened duct, and the smooth duct; the normalized values by Nu_∞ for the stationary case are 1.9, 1.7, and 1.2, respectively. As explained above, in addition to the effect of the flow separation and its reattachment between the ribs seen in the 90° rib case, the 60° rib case is also affected by the additional secondary flow induced by the angled rib. The effect of the radial flow direction on the duct-averaged heat transfer is not seen in either $Re = 10{,}000$ (not shown here) or 20,000. In Fig. 13, Nu_m slightly increases in the larger rotation number range, although it stays almost constant in the rest of the range.

4. Conclusion

When the duct rotated, the secondary flow induced by the Coriolis force affected the heat transfer which increased and decreased on the pressure and suction surfaces, respectively. Consequently, the peripheral variation of the heat transfer became larger. Installation of the 90° rib on the opposite leading and trailing walls enhanced the heat transfer and the local Nusselt number showed a streamwise periodic profile which had a local maximum between the consecutive ribs. The 60° angled rib case resulted in further enhancement of the heat transfer as compared to the 90° rib case. Judging from the local Nusselt number profile, the additional secondary flow induced by the angled rib seemed to contribute to this enhancement.

Within the present experimental conditions, the effect of the radial flow direction on the duct-averaged heat transfer was not observed because of the low Rayleigh number. The effect of the rotation number on the duct-averaged heat transfer was also very small with a slight increase in the higher rotation number range because the Coriolis induced difference of heat transfer in the opposite leading and trailing walls compensated for each other to give an almost constant duct-averaged Nusselt number irrespective of the rotation number change. On the contrary, the effect of the rib installation on the heat transfer was very large. In particular, the angled rib gave the best heat transfer performance among the configurations examined in this study.

Considering the enhanced heat transfer of the angled rib and the possible further control of heat transfer by changing the rib angle and height, the angled rib configuration seems to be prospective in the forced-convection cooling of gas-turbine blades.

Acknowledgements

The authors would like to thank Miss C. Mito and Messrs R. Kiml and S. Takeda for their assistance in performing experiments.

References

[1] B. Lakshminarayana, in: Fluid dynamics and heat transfer of turbomachinery, John Wiley & Sons, Inc., New York, 1996, pp. 597–721.
[2] S. Mochizuki, A. Murata, M. Fukunaga, Effects of rib arrangements on pressure drop and heat transfer in a rib-roughened channel with a sharp 180° turn, Trans. ASME, J. of Turbomachinery 119 (1997) 610–616.
[3] J.C. Han, P. Zhang, Effect of rib-angle orientation on local mass transfer distribution in a three-pass rib-roughened channel, Trans. ASME, J. of Turbomachinery 113 (1991) 123–130.
[4] M.E. Taslim, T. Li, D.M. Kercher, Experimental heat transfer and friction in channels roughened with angled, V-shaped, and discrete ribs on two opposite walls, Trans. ASME, J. of Turbomachinery 118 (1996) 20–28.
[5] J.W. Baughn, X. Yan, Local heat transfer measurements in square ducts with transverse ribs, Enhanced Heat Transfer ASME, HTD-Vol. 202 (1992) 1–7.
[6] S.V. Ekkad, J.C. Han, Detailed heat transfer distributions in two-pass square channels with rib turbulators, Int. J. Heat Mass Transfer 40 (11) (1997) 2525–2537.
[7] T. Bo, H. Iacovides, B.E. Launder, Developing buoyancy-modified turbulent flow in ducts rotating in orthogonal mode, Trans. ASME, J. of Turbomachinery 117 (1995) 474–484.
[8] C. Prakash, R. Zerkle, Prediction of turbulent flow and heat transfer in a ribbed rectangular duct with and without rotation, Trans. ASME, J. of Turbomachinery 117 (1995) 255–264.
[9] B.E. Launder, D.P. Tselepidakis, B.A. Younis, A second-moment closure study of rotating channel flow, J. Fluid Mech. 183 (1987) 63–75.
[10] A. Murata, S. Mochizuki, M. Fukunaga, Detailed measurement of local heat transfer in a square-cross-section duct with a sharp 180-deg turn, in: Heat Transfer 1994, Proc. of Int. Heat Transf. Conf., Brighton, GB, vol. 4, 1994, pp. 291–296.
[11] S. Mochizuki, J. Takamura, S. Yamawaki, W.-J. Yang, Heat transfer in serpentine flow passages with rotation,

Trans. ASME, J. of Turbomachinery 116 (1994) 133–140.

[12] S. Mochizuki, M. Beier, A. Murata, T. Okamura, Y. Hashidate, Detailed measurement of convective heat transfer in rotating two-pass rib-roughened coolant channels, ASME Paper, 96-TA-6, 1996.

[13] S. Mochizuki, A. Murata, W.-J. Yang, Heat transfer characteristics in a rotating square channel with radially outward/inward throughflow, in: Proc. of 5th Int. Conf. on Transport Phenomena in Rotating Machinery, Hawaii, US, vol. A, 1994, pp. 398–408.

[14] M.E. Taslim, S.D. Spring, Effect of turbulator profile and spacing on heat transfer and friction in a channel, J. of Thermophys. and Heat Transfer 8 (3) (1994) 555–562.

[15] G.J. Korotky, M.E. Taslim, Rib heat transfer coefficient measurements in a rib-roughened square passage, ASME Paper, 96-GT-356, 1996.

[16] W.M. Kays, M.E. Crawford, in: Convective Heat and Mass Transfer, 3rd ed., McGraw-Hill Inc., New York, 1993, p. 316.

[17] ANSI/ASME PTC19.1-1985 Measurement Uncertainty, Suppl on Instruments and Apparatus, Part 1, ASME Performance Test Codes, ASME 1985.

[18] W.M. Kays, M.E. Crawford, in: Convective Heat and Mass Transfer, 3rd ed., McGraw-Hill Inc., New York, 1993, p. 347.